

Modulating Barrier Properties of Stereocomplex Polylactide: The Polymorphism Mechanism and Its Relationship with Rigid Amorphous Fraction

Qi Chen, Rafael Auras, Jacob Judas Kain Kirkensgaard, and Ilke Uysal-Unalan*



Cite This: *ACS Appl. Mater. Interfaces* 2023, 15, 49678–49688



Read Online

ACCESS |



Metrics & More

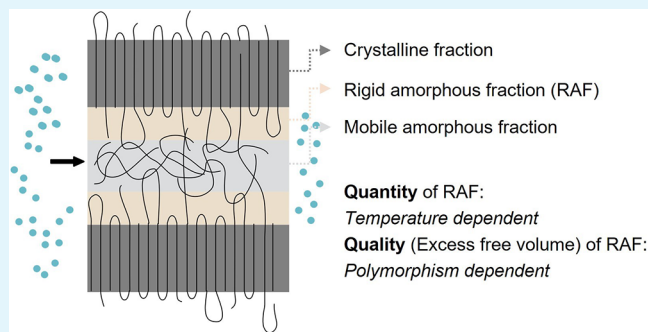


Article Recommendations



Supporting Information

ABSTRACT: The barrier properties of semicrystalline polymers are crucial for their performance and their use as packaging materials. This work uncovers the mechanism of polymorphism modification (α , α' and stereocomplex-crystals) and its combined effect on the oxygen and water vapor barrier properties of semicrystalline stereocomplex polylactide (SCPLA). A polymorphic selective filler-type nucleator was employed to eliminate the temperature effect on the development of polymorphism and rigid amorphous fraction (RAF), allowing correlations of barrier properties with different crystal forms and RAF combinations under the same amorphous composition (SCPLA). The oxygen and water vapor barrier performances strongly correlated with crystallinity and crystal form but were not monotonically related to the RAF quantity. The study proposes that the chain conformation of intermediate phases between the crystalline and amorphous phases differs with the associated crystal forms, thereby leading to different RAF “qualities” and contributing to different gas diffusion and solubility coefficients of the amorphous regions. RAF’s per unit excess free volume may be varied with crystal forms, for instance: $\alpha' \gg SC > \alpha$. Therefore, SCPLA with α' crystals exhibited high oxygen and water vapor permeabilities. Those with high SC and α crystals showed similar barrier behaviors governed by Henry’s law dissolution and followed a linear “two-phase” relationship with total crystallinity.



KEYWORDS: semicrystalline polymer, structure–property relation, gas barrier, biodegradable polymer, three-phase crystalline model

1. INTRODUCTION

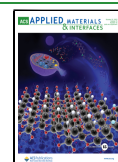
Biobased and biodegradable polylactide (PLA) is a sustainable alternative to fossil-based plastic. PLA has comparable thermal, mechanical, and barrier properties with its fossil-based counterparts; therefore, a variety of postmodification strategies have been proposed to widen its application.¹ Benefiting from the diverse polymorphism nature of PLA, one of the vital modification strategies is to manipulate the crystalline structure of PLA.² Recently, stereocomplex PLA (SCPLA), the mixture of enantiomer poly(L-lactide) (PLLA) and poly(D-lactide) (PDLA), has received intensive attention as its straightforward enhancement on the thermomechanical properties of PLA when the stereocomplex (SC) crystals are formed.^{3,4} Structural analysis by X-ray diffraction (XRD) revealed that the enhancement by SC crystals could be attributed to the higher intermolecular interaction of SCPLA than homochiral PLA (HCPLA).⁵ Regarding the barrier properties, Sangroniz et al.⁶ reported that SC crystallization incurs less rigid amorphous fraction (RAF), thereby lower excess free volume than homochiral (HC) crystallization, resulting in superior barrier performance of SCPLA material. RAF is the conformation-constrained interface between the ordered crystalline fraction (CF) and the mobile amorphous fraction (MAF) of a random

coil; RAF quantity can dictate barrier properties of semicrystalline polymers due to the distinct chain conformation than MAF.⁷ Most available research has focused on the impact of SC on RAF and barrier properties by comparing SCPLA with PLLA;^{8–10} however, the difference in amorphous composition may lead to incomplete prediction of the barrier–structure correlation.^{8,11} The capacity and mechanism of the polymorphism modification on RAF development and barrier properties in individual SCPLA have yet to be demonstrated. Not only is it critical for application as barrier packaging and medical devices, but barrier properties also act as an indication of hydrolytic degradation,¹² which is important for durable use. Therefore, understanding the polymorphism–RAF–barrier relation is pivotal for SCPLA as a sustainable plastic alternative.

Received: August 23, 2023

Accepted: September 25, 2023

Published: October 13, 2023



The structure–gas barrier relation in semicrystalline polymers has been discussed for decades,^{13,14} with one of the critical arguments about whether the two or three-phase crystalline structure model should be applied to correlate gas barrier properties with total crystallinity (equivalent to CF).^{15–17} The fundamental difference between the two models arises from the inconsistent observations of the barrier contribution from the amorphous phases. In the two-phase model, the increase of crystallinity monotonically contributes to the extended diffusion tortuous path and the reduced sorption capacity with decreased amorphous content,¹⁶ whereas the nature of the amorphous phases is neglected. However, for the three-phase model, the amorphous fraction is further specified,¹¹ for example, dividing into the RAF and MAF.⁷ The negative contribution of RAF to the barrier performance can outweigh the positive contribution of crystals. Under this situation, increasing crystallinity may fail to improve the barrier properties.¹⁶ Beyond the two and three-phase model arguments, the mixed contribution from different phases can be varied in different crystallinity ranges.¹³ Therefore, an inclusive consideration of the barrier contributions from each phase is essential. For polymorphic semicrystalline polymers, additional attention should be focused on understanding the contribution of CF. Previous work¹⁸ has revealed that polymer chains in the α , α' , and SC crystals have distinct molecular packing and dynamics, leading to different properties. As gas permeation is primarily confined within the amorphous region,^{11,14,19,20} the influence of different crystal forms on barrier properties should be realized through their impact on the amorphous regions. Moreover, in order to accurately establish the correlation between barrier properties and different crystal forms, it is essential to ensure uniformity in the composition of the amorphous regions.

Prior work by Cocca et al.²¹ assessed the barrier properties of PLLA with different α/α' ratios. Increasing the α' -crystal ratio caused an abrupt decrease in the water vapor barrier, attributed to the disordered crystal structure. However, the root mechanism of the barrier difference in α and α' crystals is still unclear, as the gas permeation occurs in the amorphous phases.¹¹ In the present work, oxygen and water vapor barrier properties of SCPLA with α , α' , and SC crystals were examined, different polymorphisms were obtained by annealing at selective temperatures, and the impact of polymorphism on amorphous phases and the barrier performances were discussed. Due to faster nucleation of SC than HC,^{22–24} most SCPLA products hold polymorphisms of exclusive SC crystals, SC + α crystals, or SC + α' crystals. Thus, this study holds fundamental insights and practical relevance for growing real-world applications of SCPLA-based materials. Additionally, a polymorphism-selective filler-type nucleator was employed to eliminate the temperature dependence of RAF and polymorphism, thereby providing an unbiased comparison of the barrier properties with different RAF contents and polymorphisms. This work provides fundamental insights into the polymorphism–RAF–barrier correlation of SCPLA-based materials to guide the design and application of sustainable products.

2. EXPERIMENTAL SECTION

2.1. Raw Materials. PLLA, trade name Luminy L130 with M_w ca. 160 kg/mol; D-lactide content <1%; PDLA, trade name Luminy D120 with M_w ca. 120 kg/mol; and L-lactide content <1% were purchased from TotalEnergies Corbion (Gorinchem, Netherlands). Layered

double hydroxide (LDH), trade name DHT-4A, and $Mg_{4.3}Al_2(OH)_{12.6}CO_3 \cdot mH_2O$, modified by fatty acid (<4%), were kindly provided by Kisuma Chemicals (Veendam, Netherlands).

2.2. Composite Film Preparation. PLLA, PDLA pellets, and LDH powder were mixed and fed into a Process 11 Parallel Twin-Screw Extruder (40/1 L/D ratio, Thermo Fisher Scientific, Massachusetts) to produce pellet-form SCPLA blends (PLLA/PDLA 1:1 in weight) with different LDH contents (0, 0.2, 0.5, and 1 wt %). The extruder temperature profile from feeder to die was 180, 220, 220, 230, 230, 240, 240, and 230 °C, and the screw speed was set at 100 rpm. The extruded pellets were then compression molded by a YLJ-HP300 heat press (MTI corporation, California) at 225 °C, 10 MPa for 5 min to produce films and then instantly quenched at ice water and collected. Immediately after quenching, compression molding was performed at 80, 140, and 200 °C and 10 MPa for 30 min to obtain annealed films with different polymorphisms. The annealed films of around 75 μ m thickness were further characterized. The films treated at 225 °C for 5 min are labeled as T_{225} , and the films treated further at 80, 140, and 200 °C for 30 min are labeled as T_{80} , T_{140} , and T_{200} , respectively. The neat SCPLA films are named SCPLA, and the SCPLA/LDH composite films with x wt % LDH loading are named xLDH. Amorphous films were made to estimate the heat capacity change of amorphous SCPLA by compression molding the pellets at 250 °C, 10 MPa for 5 min and then instantly quenching in ice water.

2.3. Modulated Differential Scanning Calorimetry (MDSC). MDSC (Q2000, TA Instruments, New Castle) was employed to characterize the heat capacity of the annealed film, and the measurements were conducted with a modulation amplitude of ± 0.318 °C, a period of 60 s, and a heating rate of 2 °C/min. The data from 10 to 100 °C were used to calculate the heat capacity for estimating the MAF fraction. The instrument was calibrated with indium and sapphire standards, and 5.5 ± 0.5 mg of annealed films was weighed for all measurements.

2.4. Small/Wide-Angle X-ray Scattering (SWAXS). The polymorphism, crystallinity (CF), and crystalline structure of the annealed SCPLA and its LDH composite films were analyzed by SWAXS using a Nano-inXider ($\lambda = 0.154$ nm, Xenocs, Sassenage, France) operated at 50 kV, 0.6 mA, and beam size 800 μ m within a q range from 0.01 to 4 \AA^{-1} .

2.5. Oxygen and Water Vapor Barrier Properties. Oxygen and water vapor transmission rates (OTR and WVTR) of the annealed SCPLA and its LDH composite films were measured on a 2 cm^2 surface sample using an XS/Pro-Totalperm permeability analyzer (Extrasolution Srl, Capannori, Italy) equipped with an electrochemical sensor. The OTR was measured according to ASTM F2622, with a carrier flow (N_2) of 10 mL/min at 23 °C, 50% relative humidity (RH), and 1 atm pressure difference on the two sides of the specimen. The water vapor transmission rate was measured with a carrier flow (N_2) of 10 mL min^{-1} at 38 °C, 90% RH, and 0.06 atm pressure difference on the two sides of the specimen according to ASTM F 1249. Each of the OTR and WVTR values had an average of at least two replicates. To eliminate any influence arising from different film thicknesses, OTR [$(\text{cm}^3/(\text{m}^2 \cdot 24\text{h}))$] and WVTR [$(\text{g}/(\text{m}^2 \cdot 24\text{h}))$] values were converted to permeability coefficients P_{O_2} [$(\text{kg}\cdot\text{m}/(\text{m}^2 \cdot \text{s} \cdot \text{Pa}))$] and P_{H_2O} [$(\text{kg}\cdot\text{m}/(\text{m}^2 \cdot \text{s} \cdot \text{Pa}))$], respectively.

3. RESULTS AND DISCUSSIONS

WAXS was used to examine the polymorphism of the resulting SCPLA and its LDH composite films after annealing at different temperatures. Figure 1 shows the WAXS patterns of neat SCPLA films obtained from different annealing temperatures (80, 140, 200, and 225 °C). The WAXS and normalized WAXS patterns of SCPLA and LDH-filled SCPLA samples are provided in Figures S1 and S2, respectively. The detailed annealing procedure is described in the Section 2. Samples annealed at 225 °C (T_{225}) showed three subtle diffractions at around $2\theta = 12.0$, 21.0, and 24.0° (red dash lines in Figure 1),

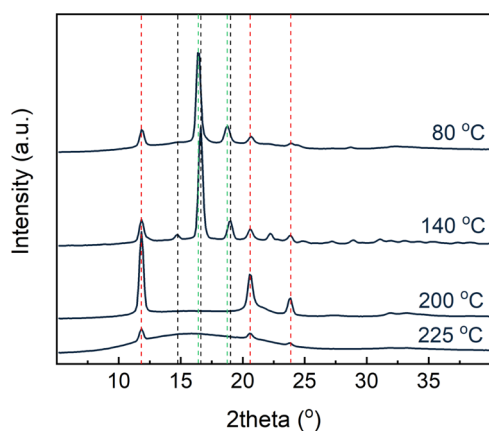


Figure 1. WAXS patterns of neat SCPLA films obtained after annealing at different temperatures. The dashed lines guide the eyes for selective diffraction peaks. The red dashed lines represent SC form, the black dashed line represents the α crystals, and the green dashed lines represent the α' crystals.

corresponding to the 110, 300/030, and 200 crystal planes of the SC crystals.^{4,25} Similarly, samples annealed at 200 °C (T_{200}) also showed an exclusive SC crystal with sharper diffraction peaks, indicating a higher SC crystallinity obtained at 200 °C. While 225 and 200 °C annealing led to exclusive SC crystallization, WAXS showed that the samples annealed at 140 °C (T_{140}) and 80 °C (T_{80}) developed a low SC fraction polymorphism, originating from the film-making process at 225 °C by heat press. In addition to the small content of SC crystals, T_{140} showed major diffraction peaks at 14.8, 16.6, and 19.0° (black dash lines in Figure 1) associated with the 010, 110/200, and 203 crystal planes, respectively, of the α crystals.^{25,26} The WAXS pattern of T_{80} and T_{140} seemed very similar at first glance; however, in T_{80} , a weak peak at around 14.8° was not observed and a shift of two peaks at around 16.6 and 19.0° took place, indicating an exclusive α' -crystal growth in the presence of preformed SC crystals.²⁶ So, based on WAXS, T_{225} and T_{200} correspond to samples with an exclusive SC-crystal polymorphism, and T_{140} and T_{80} correspond to samples with a primary α -crystal and α' -crystal polymorphism, respectively.

The WAXS-based crystallinity of samples obtained from different annealing temperatures is shown in Figure 2, and the values are included in Table S1. The crystallinity was calculated by the ratio of the areas of crystalline peaks and the area of the whole diffraction pattern. The area of crystalline peaks was determined by the area of the peaks after subtracting the amorphous halo obtained from amorphous SCPLA annealed at 250 °C.²⁷ Like in the discussion above, T_{225} and T_{200} generated exclusive SC content. Due to the selective SC nucleation effect by LDH,²⁸ increasing LDH content to ≥ 0.5 wt % resulted in a higher SC crystallinity compared to lower LDH content. For T_{140} and T_{80} samples, 0.5 and 1 wt % LDH loading (0.5LDH and 1LDH) altered the polymorphism toward higher SC-crystal content, whereas less LDH content yielded HC-dominated polymorphism.

Figure 3 shows the oxygen and water vapor permeabilities of SCPLA and its LDH composites with different polymorphism modifications; the data are reported in Table S1. The corresponding crystal forms were marked in legends and for samples with polymorphism, the values of SC fraction (ratio of SC crystallinity to total crystallinity) were denoted by circle symbols. As reported elsewhere, LDH may weaken the thermal stability of PLA.²⁹ However, in the present study, the correlation between polymorphism obtained by different annealing temperatures and barrier properties remained consistent at different LDH contents, indicating that the possible molecular weight reduction of PLA did not alter the polymorphism–barrier correlation. Future work should further assess this parameter. On the other hand, unlike the oxygen molecules, water molecules clustering could occur during the water vapor transport in polymers, causing plasticization in the polymer matrix and increased permeant effective size.^{30,31} However, changing the annealing temperatures had the same trend of impact on the oxygen and water vapor permeability values in the present study. Though the water permeation mechanism of PLA is still in debate,^{21,32–34} the similar trend in Figure 3B as A implies that water molecules in this study followed the sorption–diffusion mechanism as oxygen molecules did. In this regard, the permeant was strictly confined in the amorphous regions and bypassed the crystals during transport, leading to a parallel increase of the tortuous path and a decrease of the sorption site with crystallinity.¹⁴ It

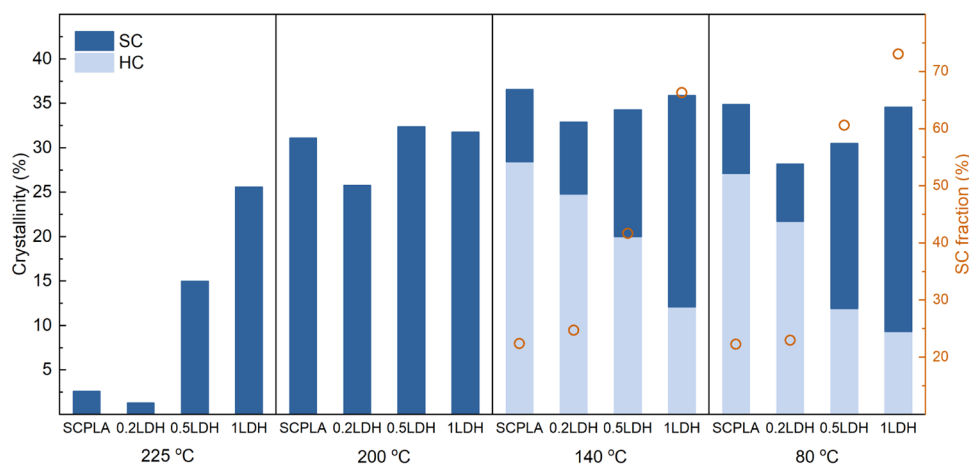


Figure 2. SC, HC crystallinity (denoted in the legend) of SCPLA and its LDH composite films after annealing at different temperatures (marked on the X-axis). For polymorphic samples obtained from annealing at 140 and 80 °C, the SC fraction (ratio of SC crystallinity to total crystallinity) is denoted by yellow circles.

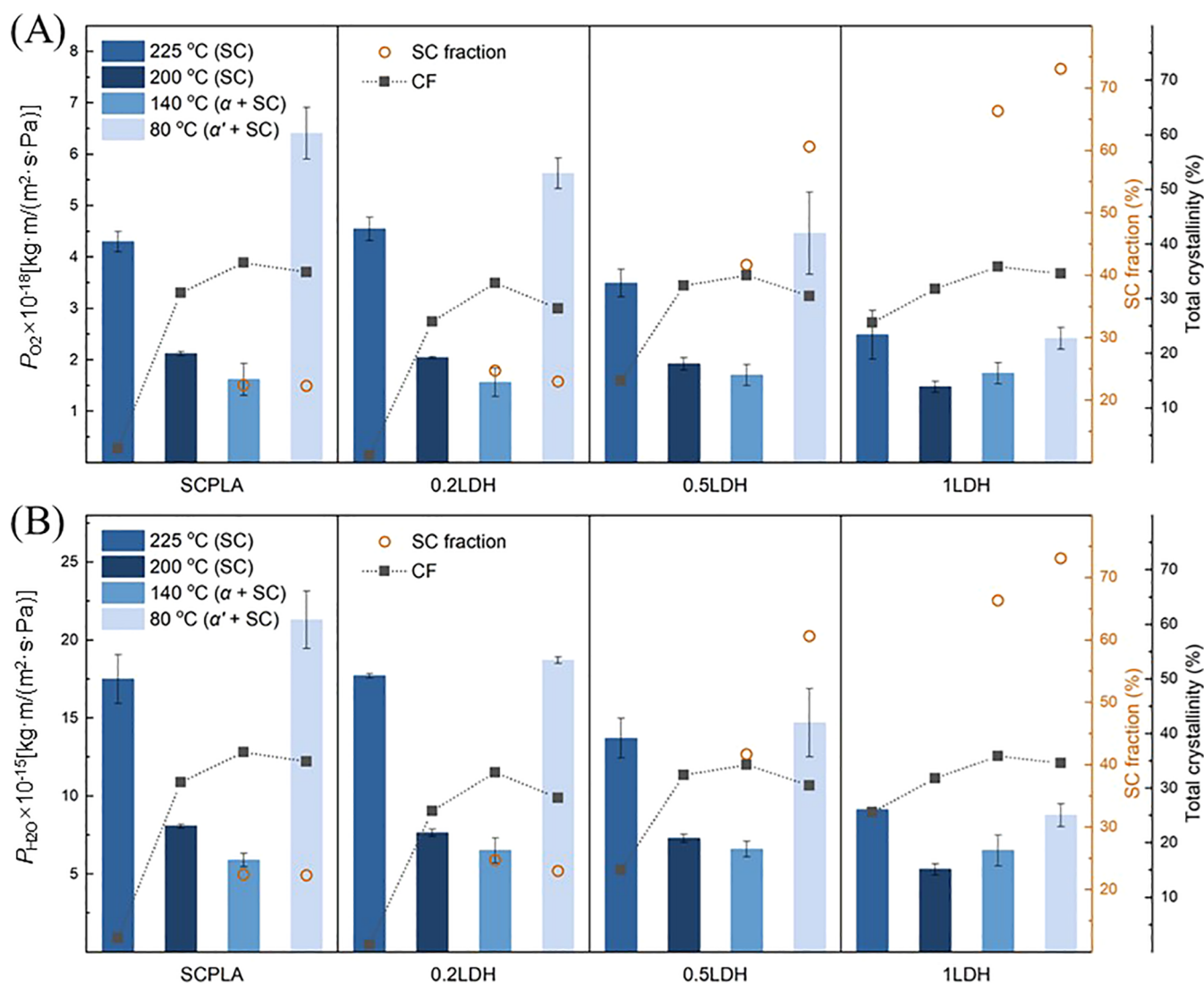


Figure 3. (A) Oxygen and (B) water vapor permeability of SCPLA and its LDH composites with different polymorphism modifications after annealing at different temperatures, as denoted in the legend. The SC, $\alpha + \text{SC}$, and $\alpha' + \text{SC}$ mark the “exclusively SC”, “primarily α ”, and “primarily α' ” polymorphisms of the corresponding samples, respectively. For polymorphic samples obtained from annealing at 140 and 80 °C, the SC fraction (ratio of SC crystallinity to total crystallinity) is denoted by yellow circles.

was also observed that sufficient crystallinity should be established for barrier improvement related to the space-filling of crystals.¹³ Therefore, among samples with different polymorphisms, T_{225} samples with low crystallinity showed less oxygen and water vapor barrier than did the T_{140} and T_{200} samples with higher crystallinity. T_{80} samples, on the other hand, displayed significantly higher permeability values than T_{140} and T_{200} samples and even the nearly amorphous T_{225} samples for those with 0, 0.2, and 0.5 wt % LDH. The high oxygen/water vapor permeabilities of T_{80} samples at much higher crystallinities than T_{225} demonstrate that α' crystals deteriorated the barrier properties, compensating for the positive effect of the increased crystallinity. Since crystals are impermeable to gases, this indicates that the amorphous regions associated with α' crystals are more permeable compared to those associated with T_{225} , at even lower content (1-CF). The underlying mechanism for this phenomenon is elaborated on in later sections.

As the similar SC crystallinity between 1LDH at T_{225} and T_{80} , it can be deduced that, in T_{80} samples, the SC crystal was

formed mainly during the film-making at 225 °C, and the α' crystals were formed afterward during the 80 °C annealing. Given the similarity of crystallinity for T_{80} , T_{140} , and T_{200} samples, this implies that postdecoration of α' crystals onto samples with the SC crystals deteriorated barrier performance. Additionally, the negative contribution gradually decreased with a lower α' -crystal fraction. Such a phenomenon was also observed by Cocca et al.²¹ in PLLA, where α' modification on α crystals leads to an abrupt increase in water vapor permeability. The present study first reports the combined polymorphism effect on barrier properties between α' and SC crystals. Likewise, it is possible that the coexistence of α and SC crystals rather than the α crystals alone resulted in exceptional barrier performance in T_{140} samples via a combined effect, yet varying SC fractions showed little influence. Tsuji and Tsuruno⁸ reported that the barrier properties of SC-crystallized SCPLA were found to be better than α -crystallized HCPLA in a wide range of crystallinity from 0 to 40%, which was mainly associated with the different amorphous compositions of PLLA and SCPLA, where the high

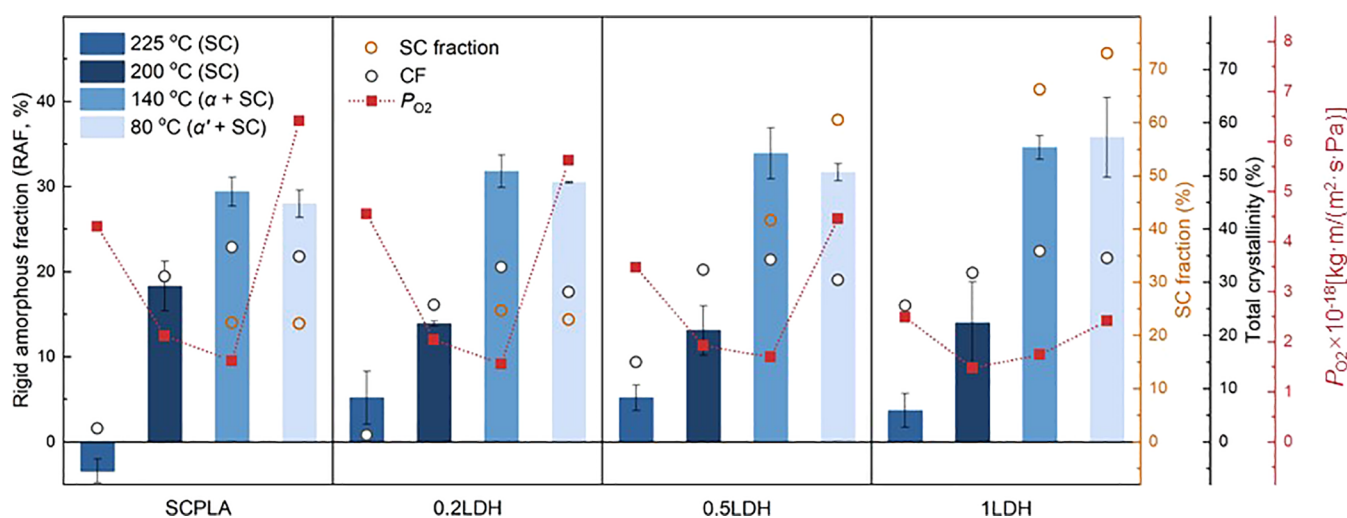


Figure 4. RAF of SCPLA and its LDH composites with different polymorphism modifications after annealing at different temperatures, as denoted in the legend. The SC, α + SC, and α' + SC mark the “exclusively SC”, “primarily α ”, and “primarily α' ” polymorphisms of the corresponding sample, respectively. For polymorphic samples obtained from annealing at 140 and 80 °C, the values of the SC fraction (ratio of SC crystallinity to total crystallinity) are denoted by yellow circles.

interaction between enantiomers delays the gas permeation. The mechanism of polymorphism modification on the barrier properties of SCPLA with the same amorphous composition and the combined effect between different crystal forms are discussed in the next section.

As stated, the failure of applying a two-phase semicrystalline structure model with a sole focus on the crystallinity values to evaluate the relationship between the microstructure and barrier properties of semicrystalline polymers has often been observed, revealing the incomplete prediction of barrier performance. Therefore, the concept of RAF as an intermediate phase positioned between the amorphous and crystalline phases has been introduced to explain the two-phase model failure. In fact, related studies conducted comprehensive quantification considering that the RAF^{6,31} is very limited and sometimes contradictory. The seemingly straightforward statement from the existing findings that the RAF is the sole factor in predicting barrier properties rests on a basic assumption. There is, however, a need for more inclusive and comprehensive research to understand the impact of the relationship of RAF–polymorphism on the barrier performance of semicrystalline polymers. In the present study, the RAF was calculated by eq 1

$$\text{RAF} = 1 - \text{MAF} - \text{CF} \quad (1)$$

where MAF can be estimated by the ratio of heat capacity change (ΔC_p) during the glass transition of samples to that of the amorphous film samples annealed at 250 °C for 5 min, as described in the Section 2. The WAXS-based CF values were chosen, and the calculated RAF results are presented in Figure 4. The CF, MAF, and RAF values are summarized in Table S1.

Annealing temperature significantly affected the RAF formation of SCPLA and its LDH composite films. T_{225} resulted in RAF lower than 5%, with the exclusive SC crystallinity below 25%. The subzero values of RAF originated from the slight underestimation of the ΔC_p of the fully amorphous-state SCPLA by using the values obtained from SCPLA annealed at 250 °C. This could be because of local chain ordering, prompted by the nucleation tendency that might take place during the quenching from 250 °C. Although

WAXS detected no crystal diffraction, it may lead to lower ΔC_p values compared to the ideally fully amorphous SCPLA. As a result, the MAF may be overestimated due to the underestimated ΔC_p , and consequently, the RAF, calculated as $1 - \text{MAF} - \text{CF}$, could be underestimated. Introducing LDH had little effect on the RAF of T_{225} and T_{200} samples but led to a gradual increase of RAF for T_{140} and T_{80} samples. In our previous work,²⁸ it was found that LDH below 1 wt % loading does not introduce the filler-induced RAF but the local nucleation-induced ordering effect could cause an increase of overall RAF quantity, as evidenced in T_{140} and T_{80} . The independence of RAF from LDH loading at T_{225} and T_{200} indicates that the nucleation-induced RAF may not develop at such high temperatures with high chain mobility.

Notably, samples with α (T_{140}) and α' (T_{80}) crystals rendered similar RAF quantity that was higher than samples with exclusive SC (T_{225} and T_{200}). For nearly amorphous samples at T_{225} , this may be because RAF may develop only when sufficient geometrical constraints and crystallinity are established, as observed in Fernandes-Nassar’s work,¹⁹ where RAF drastically increased from 3 to 35% when the spherulites impingement occurred after the CF increased from 17 to 35%. However, T_{200} samples hold comparable CF but lower RAF as compared with T_{140} and T_{80} . This may relate to the polymorphism-dependent RAF development behavior,^{35,36} and in Sangroniz et al.’s⁶ work was attributed to the high chain decoupling capacity during the SC crystallization. As the paired enantiomer segments are excluded from the amorphous region during crystallization, a high free volume may develop, which enables a more complete chain decoupling and lower RAF development than HC crystallization. However, comparing 0.2LDH with 1LDH samples, variations in SC fraction did not obviously alter the RAF quantity at T_{140} or T_{80} . In contrast, T_{225} consistently showed the lowest RAF quantity even the comparable CF of 1LDH at T_{225} with 0.2LDH at T_{200} , which can be attributed to the high chain mobility and decoupling capacity during crystallization at high temperatures, as previously revealed by time-resolved MDSC and flash-DSC techniques.^{37,38} In summary, the independence of the SC-crystal fraction with RAF quantity supports the hypothesis that

RAF is not built up with sufficient chain mobility at high temperatures and demonstrates that in the SCPLA system, the RAF quantity is temperature-dependent rather than polymorphism-dependent. Accordingly, the MAF ($1 - CF - \text{RAF}$), consisting of amorphous chains that did not vitrify into crystal or RAF regions, is also dependent on temperature, which influences the crystallization rate and the development of RAF. For instance, SCPLA at T_{200} has a higher MAF value than that at T_{80} for similar CF, suggesting that more RAF was developed in the SCPLA samples at T_{80} .

For a given semicrystalline polymer, it is believed that, at a constant CF, higher RAF yields lower gas barrier performance.¹⁹ Concerning the RAF–barrier correlation in SCPLA, as shown in Figure 4, at similar CF, T_{200} with a significantly lower RAF content showed a similar oxygen barrier performance with T_{140} . In contrast, T_{140} and T_{80} , with similar RAF contents, exhibited significantly different barrier performances. This means that the RAF quantity alone cannot be the decisive and dominating factor for the barrier performance of the polymorphic SCPLA system, even at similar crystallinity. To further understand the structure–barrier relation in the SCPLA system, Figure 5 shows the oxygen barrier and total

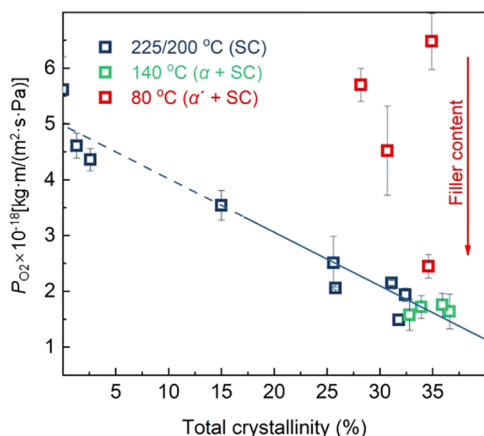


Figure 5. Unbiased correlation between oxygen permeability and total crystallinity (CF) of all SCPLA and its LDH composites in the present study after annealing at different temperatures. The blue dashed line represents an extrapolated linear correlation between oxygen permeability and crystallinity, and the red arrow indicates the increase of filler content for samples annealed at 80 °C. The polymorphism is labeled in the legend and the SC, $\alpha + \text{SC}$, and $\alpha' + \text{SC}$ mark the “exclusively SC”, “primarily α ”, and “primarily α' ” polymorphism of the corresponding sample, respectively.

crystallinity correlation for all samples in the present study. Interestingly, the barrier–crystallinity correlation for samples with exclusive SC crystals (T_{225} , T_{200}) and α crystals (T_{140}) followed a linear, “two-phase” model, whereas the samples with α' crystals (T_{80}) behaved differently and fell out of the linear correlation. Increasing the LDH content to 1 wt % halved the oxygen permeability of T_{80} samples but had less impact on the samples with an exclusive SC (T_{225} and T_{200}) or α crystal (T_{140}), which probably reached the barrier limit under the corresponding polymorphism and crystallinity. Notably, when 1 wt % LDH was loaded, the polymorphism of T_{80} samples was altered to a high SC crystal, and the barrier–crystallinity correlation fell into the linear region. This behavior demonstrates the strong correlation between polymorphism and barrier properties of SCPLA. Meanwhile, the linear

correlation of barrier–crystallinity for SCPLA with exclusive SC and α crystals suggests that the structural variations in the amorphous phase, signified by the RAF ratio in amorphous phases, did not substantially alter the barrier performance. Since the existence of the intermediate phase, RAF, is evident, it is critical to understand the possible mechanism of this unique structure–barrier correlation in the SCPLA system.

As previously mentioned, modifying the annealing temperatures and LDH content generated a parallel pattern in terms of its effect on the permeability of both oxygen and water vapor in the present study (Figure 3). Despite ongoing discussion concerning the precise mechanism of water permeation within PLA,^{21,32–34} the analogous trend observed in oxygen and water vapor permeabilities suggests that the water molecules followed the same sorption–diffusion mechanism as their oxygen counterparts in this work. Therefore, the permeability coefficient P , diffusivity coefficient D , and solubility coefficient S can be described by eq 2.

$$P = DS \quad (2)$$

For the two-phase and three-phase models, the crystals are considered impermeable, and thereby, the gas sorption and diffusion are strictly limited to the amorphous phase. Consequently, the nature of the amorphous phase, such as conformation, chain defects, segmental dynamics, and excess free volume, plays a crucial role in determining D and S . The D of the semicrystalline polymer can be described by eq 3²⁰

$$D = \frac{D_a}{\tau\beta} \quad (3)$$

where D_a is the diffusivity coefficient of a completely amorphous polymer, τ represents the tortuosity factor of the diffusion path, and β is the impedance factor reflecting the ability to trap permeant motion by the intermediate phases near crystals.²⁰ The sorption behavior in the semicrystalline polymer can be characterized by the dual-model sorption,^{39–41} where the solubility coefficient is represented by eq 4

$$S = k_D + \frac{c'_H b}{1 + bp} \quad (4)$$

k_D is the Henry’s Law constant, representing the contribution from the dissolution following Henry’s law, where the sorption behavior resembles the gas dissolution into liquid or rubbery polymers.⁴¹ k_D is dependent on the thermodynamic interaction between the gas and the polymer.⁴² The latter part denotes the contribution from Langmuir-type sorption where the sorption occurs within “microvoids”.^{43,44} p is pressure, c'_H is the Langmuir capacity related to the excess free volume, and b is the Langmuir affinity parameters.⁴¹ For semicrystalline polymers characterized by the three-phase structure, the contribution of amorphous phases to β and c'_H , as indicated by changes in D and S , should be determined by the nature of the amorphous phases, including chain conformation and composition of RAF and MAF.

A unique feature of polymorphic systems is the distinct chain packing within different crystal forms. Pan et al.¹⁸ investigated the molecular packing and dynamics in the α , α' , and SC crystals. The α' crystals were found to have a disordered conformation and loose lateral packing, while in the α and SC crystals, the dipolar interactions and hydrogen bonding enable a tighter chain packing. Figure 6 shows the Lorentz-corrected SWAXS curves for SCPLA with different

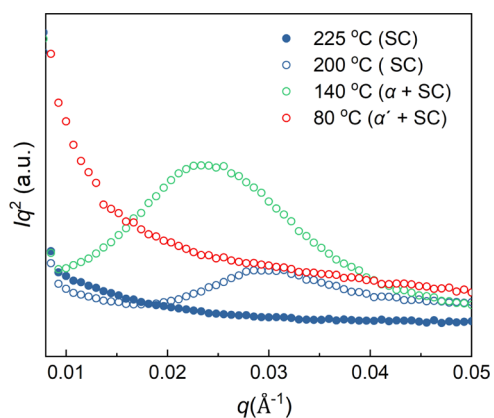


Figure 6. SAXS profiles of SCPLA with different polymorphism modifications after annealing at different temperatures. The polymorphism is labeled in the legend, and the SC, α + SC, and α' + SC mark the “exclusively SC”, “primarily α ”, and “primarily α' ” polymorphisms of the corresponding sample, respectively.

polymorphisms. The T_{200} and T_{140} showed distinguishable long-period maxima in the SAXS profile, standing for the periodic lamella structure of the SC/ α crystal and the sharp interface between crystalline and amorphous phases. On the other hand, T_{225} with low crystallinity and T_{80} with an α' crystal exhibited diffuse and broad scattering, which is an indication of the low electronic density difference between the crystalline and amorphous phases. The diffuse SAXS pattern of the α' crystal, even with the periodic lamellae structure, has been observed in other studies as well.^{45–47} For example, Diez-Rodríguez et al.⁴⁵ found that in samples annealed at 75 °C, which developed a primary α' crystal, no long-spacing peak was detected. This diffuse SAXS pattern without the long-spacing maximum in the α' crystal can be ascribed to the conformational disorder,^{18,46,48} where partial chains in the unit cell of the α' crystal may adopt the helix conformation other than 10_3 as the most do and distribute randomly in the unit cell.^{26,49} Such a disorder could decrease the electronic density difference between the crystalline and amorphous phases, showing a diffuse SAXS pattern.⁴⁶ Despite this disorder, the chain packing within the α' crystal remains sufficiently

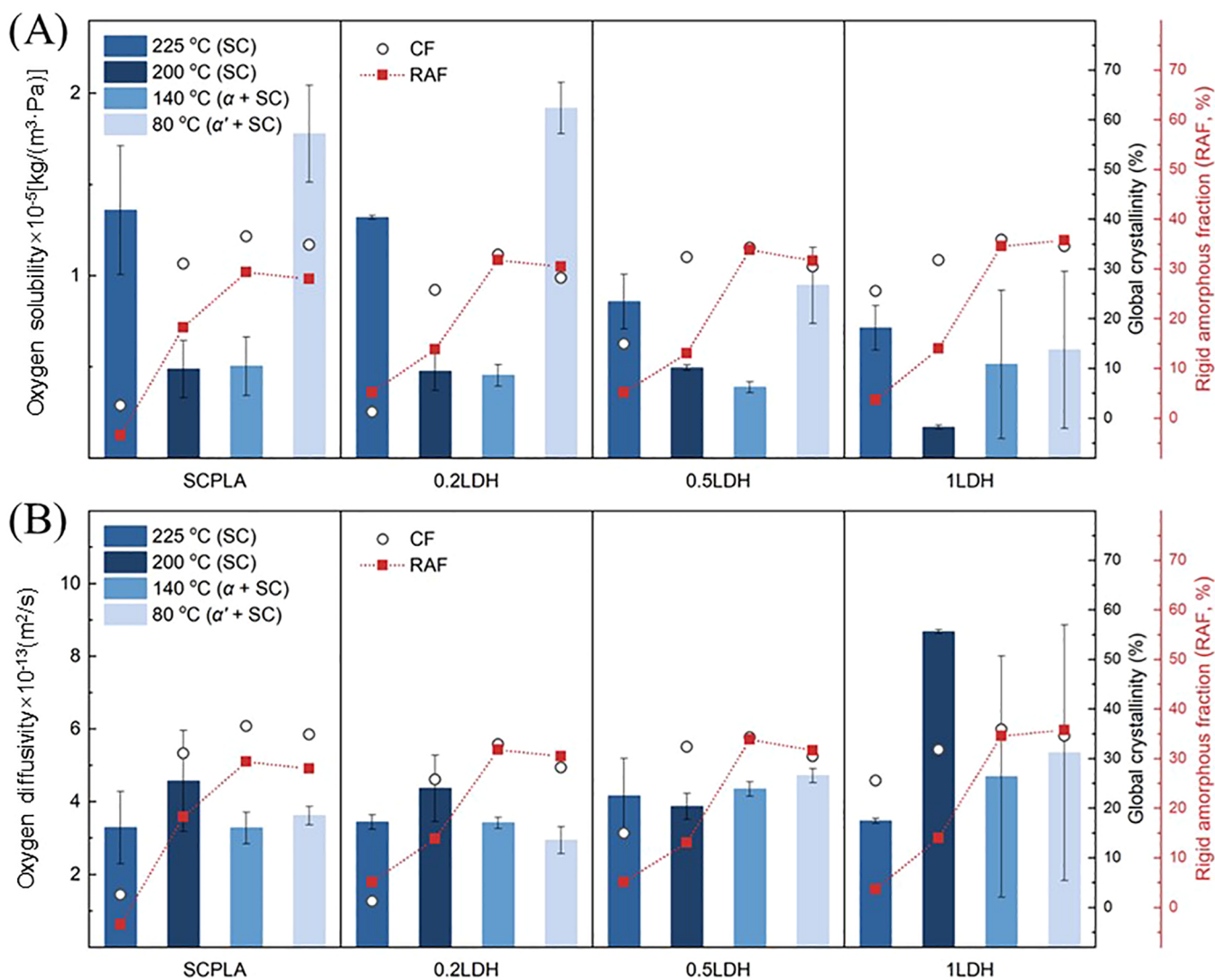


Figure 7. Oxygen solubility (A) and diffusivity (B) of SCPLA and its LDH composites with different polymorphism modifications after annealing at different temperatures, as denoted in the legend. The SC, α + SC, and α' + SC mark the “exclusively SC”, “primarily α ”, and “primarily α' ” polymorphisms of the corresponding sample, respectively.

compact to be impermeable to gas molecules. In fact, the α' crystal possesses similar unit cell parameters ($a = 10.80 \text{ \AA}$, $b = 6.20 \text{ \AA}$, $c = 28.80 \text{ \AA}$) as the α crystal ($a = 10.683 \text{ \AA}$, $b = 6.170 \text{ \AA}$, $c = 28.860 \text{ \AA}$).^{48,50} However, given the similar CF and RAF quantities in T_{80} and T_{140} samples, it is rational to propose that the nature of amorphous phases, especially regions anchored onto the lamella surface, differs depending on the crystal forms. In fact, the nature of amorphous or intermediate phases has been found to be variable, for example, holding restricted mobility and rendering low water vapor transmission,⁸ tailorable free volume and barrier properties by low molecular weight compound,¹¹ holding a continuum of mobility,⁵¹ and showing polymorphism-dependent RAF quantity and thermal properties.^{35,36} Hence, while the random enantiomer chains in MAF may have the same properties, RAFs associated with α' , α , and SC crystals (denoted by $\text{RAF}_{\alpha'\text{-crystal}}$, $\text{RAF}_{\alpha\text{-crystal}}$, and $\text{RAF}_{\text{SC-crystal}}$) may hold different chain conformations and excess free volume, thereby contributing differently to the β and c_H' values; consequently, the different D and S can serve as an insight of difference in the excess free volume.

To ascertain the excess free volume of RAF associated with different polymorphisms and its impact on the barrier behavior of SCPLA, the D of films was first estimated by fitting the experimental gas transmission rate curves with eq 5, as described in previous works.^{6,32,52}

$$\frac{F_t}{F_\infty} = \left(\sqrt{\frac{l^2}{4Dt}} \right) \sum_{n=1,3,5}^{\infty} \exp\left(-\frac{n^2 l^2}{4Dt} \right) \quad (5)$$

where F_t and F_∞ are the gas transmission rate at time t and steady state, respectively, and l is the film thickness. The representative plots of experimental and fitted curves as a function of time are provided in Figure S3 of the Supporting Information. Consequently, the S of films can be obtained by solving eq 2, where $P = DS$. Figure 7 shows the oxygen diffusivity and solubility coefficients of SCPLA and its LDH composites. The coefficients of water vapor are in a similar trend and are shown in Figure S4. It can be found that increasing the LDH content in T_{225} and T_{80} samples significantly altered the solubility rather than the diffusivity, which indicates that LDH itself did not substantially contribute to the tortuosity path within the studied range. The improved permeability was the consequence of increased crystallinity or altered polymorphism induced by the selective nucleation effect of LDH. Notably, altering polymorphism hardly affected the diffusivity either, which means that the permeation was primarily sorption-controlled progress. While the polymorphism effect on D was revealed to be negligible, the polymorphism obviously affected the S .

For a given matrix of SCPLA and gases (oxygen or water vapor), Henry's Law constant k_D and Langmuir affinity parameter b should remain constant.⁵³ As such, according to eq 4, the S values should be proportional to the excess free volume ($S \propto c_H'$). Consequently, as indicated in Figure 7, at similar CF and RAF, samples with α' crystals demonstrated high S values that could be ascribed to the high excess free volume in the $\text{RAF}_{\alpha'\text{-crystal}}$ formed near the disordered α' -lamella surface. This implies that polymorphism may exert different properties on the RAF through different excess free volumes, which may relate to the different chain packing habits in lamellae; however, more quantification analysis for free volume should be conducted to estimate further the RAF associated with different crystal forms in more semicrystalline

polymers. In the present study, we may propose that per unit of $\text{RAF}_{\alpha'\text{-crystal}}$ has lower excess free volume than $\text{RAF}_{\text{SC-crystal}}$ resulting from that at similar crystallinity (30–35%) in the T_{140} and T_{200} samples, the quantity of $\text{RAF}_{\alpha'\text{-crystal}}$ (around 33%) is about twice of $\text{RAF}_{\text{SC-crystal}}$ (around 15%); however, the S values of T_{140} and T_{200} samples are similar.

Additionally, for the samples with exclusive SC (T_{225} , T_{200}) and α crystals (T_{140}), the sorption behavior governed the barrier performance demonstrating a linear correlation between S and crystallinity and the unpronounced changes of D values (Figure S5). Specifically, as the variations of amorphous regions (RAF) in these T_{200} and T_{140} samples with similar crystallinity did not significantly change the barrier behaviors, the sorption may be governed by Henry's law dissolution. This could be because both $\text{RAF}_{\text{SC-crystal}}$ and $\text{RAF}_{\alpha\text{-crystal}}$ have relatively low excess free volume, thereby weak Langmuir-type sorption (low c_H').^{44,54} As discussed above, T_{200} samples with an exclusive SC-crystal form had lower RAF but held similar barrier properties with T_{140} samples with α crystals and higher RAF content; the excess free volume per unit of RAF may follow: $\text{RAF}_{\alpha'\text{-crystal}} \gg \text{RAF}_{\text{SC-crystal}} > \text{RAF}_{\alpha\text{-crystal}}$. Consequently, this could explain the possible mechanism of the observed combined polymorphism effect on the barrier properties of systems with multiple crystal forms. This remarkably high excess free volume associated with α' crystals deteriorated the barrier properties of samples by offering microvoids,^{6,55} thereby showing an obvious negatively combined effect when the α' crystals formed aside with SC and α crystals. When the fraction of α' crystals is very low, the deterioration impact of α' crystals can be neglected, as in the cases of 1LDH, T_{80} samples. As for the combination of SC and α crystals, on the other hand, these two crystal forms may generate RAF with slightly different quantities but low excess free volume; therefore, the variations in the SC/ α -crystal ratio had little effect on excess free volume, resulting in a less pronounced influence on barrier properties, as in the cases of T_{200} and T_{140} samples. Future works, including positron annihilation lifetime spectroscopy techniques, can also verify the impact of polymorphic changes on the free volume of RAF on the transport properties of a wide range of semicrystalline polymers.

4. CONCLUSIONS

In the present study, SCPLA with various α , α' , and SC polymorphisms was obtained by implementing the annealing process at different temperatures. The polymorphism, crystallinity, and RAF content of the samples were quantitatively analyzed by MDSC and WAXS. To correlate these properties with oxygen and water vapor barrier performances, the temperature effect on polymorphism and RAF development was eliminated with the aid of a polymorphism-selective nucleator, LDH. The results showed that SCPLA with exclusive SC crystals obtained by annealing at 200 °C presented a similar barrier property as the SCPLA with α crystals obtained by annealing at 140 °C. In contrast, SCPLA with α' crystals obtained by annealing at 80 °C demonstrated much worse barrier performance than a solely SC crystal or combined SC/ α crystal polymorph-included samples. Additionally, barrier properties indicated a strong correlation with total crystallinity for the SCPLA with SC or SC/ α polymorphism, unlike the sample annealed at 80 °C with SC/ α' polymorphism. This was manifested by introducing the polymorphism-selective nucleator LDH into SCPLA. As the

LDH concentration of annealed samples at 80 °C increased from 0 to 0.5 wt %, SC-crystal fractions in the samples gradually increased and later became dominating when the polymer reached its maximum LDH content, leading the sample to fall into the linear region of the barrier–crystallinity correlation. Another factor, RAF, mostly known for its detrimental gas barrier impact, was found depending on crystallization temperature rather than polymorphism. However, though the permeation should follow a sorption–diffusion mechanism in the amorphous phases, barrier performances were observed to have less reliance on the RAF quantity. We propose that both RAF quantity and “quality” are crucial for the barrier performance of the semicrystalline polymer. The RAF “quality”, signified by the per unit excess free volume, should be related to the associated crystal form. Consequently, the *S* and *D* coefficients results suggest that per unit excess free volume in RAF associated with α and SC crystals is much less than that of α' crystals. Therefore, the SCPLA with the α' crystal-dominated polymorphism showed exceptionally high permeabilities, and SCPLA with α and SC crystal-dominated polymorphisms presented the linear crystallinity–permeability correlation where the barrier properties were dominated by Henry’s law dissolution. This work demonstrated a possible mechanism of using polymorphism to modify the barrier properties of SCPLA systems, and this proposed mechanism is anticipated to expand other semicrystalline polymers with the motivation of raising awareness about biobased polymers and increasing demand for high-barrier sustainable solutions.

■ ASSOCIATED CONTENT

SI Supporting Information

The Supporting Information is available free of charge at <https://pubs.acs.org/doi/10.1021/acsami.3c12602>.

WAXS patterns of SCPLA/LDH composite films obtained after annealing at different temperatures; normalized WAXS patterns of SCPLA and its LDH composite films obtained after annealing at different temperatures; HC crystallinity, SC crystallinity, crystal fraction, mobile amorphous fraction, rigid amorphous fraction, oxygen permeability, and water permeability of SCPLA and its LDH composites; plots of experimental and fitted permeation curves as a function of time; water vapor solubility and diffusivity of SCPLA and its LDH composites with different polymorphism modifications; and solubility and diffusivity of stereocomplex polylactide at various crystallinities (PDF)

■ AUTHOR INFORMATION

Corresponding Author

Ilke Uysal-Unalan – Department of Food Science, Aarhus University, 8200 Aarhus N, Denmark; CiFOOD – Center for Innovative Food Research, Aarhus University, 8200 Aarhus N, Denmark; orcid.org/0000-0002-0963-6166; Email: iuu@food.au.dk

Authors

Qi Chen – Department of Food Science, Aarhus University, 8200 Aarhus N, Denmark; CiFOOD – Center for Innovative Food Research, Aarhus University, 8200 Aarhus N, Denmark; orcid.org/0000-0002-6908-0040

Rafael Auras – School of Packaging, Michigan State University, East Lansing, Michigan 48824-1223, United States; orcid.org/0000-0002-4378-359X

Jacob Judas Kain Kirkensgaard – Department of Food Science, University of Copenhagen, 1958 Frederiksberg C, Denmark; Niels Bohr Institute, University of Copenhagen, 2100 Copenhagen Ø, Denmark; orcid.org/0000-0001-6265-0314

Complete contact information is available at: <https://pubs.acs.org/doi/10.1021/acsami.3c12602>

Notes

The authors declare no competing financial interest.

■ ACKNOWLEDGMENTS

This work was supported by CiFOOD—Centre for Innovative Food Research at Aarhus University (AU). Data were generated by accessing research infrastructure at Aarhus University and the University of Copenhagen, including FOODHAY (Food and Health Open Innovation Laboratory, Danish Roadmap for Research Infrastructure). The authors also thank Kisuma Chemicals for generously supplying LDH.

■ REFERENCES

- (1) Castro-Aguirre, E.; Iñiguez-Franco, F.; Samsudin, H.; Fang, X.; Auras, R. Poly(Lactic Acid)—Mass Production, Processing, Industrial Applications, and End of Life. *Adv. Drug Delivery Rev.* **2016**, *107*, 333–366.
- (2) Zheng, Y.; Pan, P. Crystallization of Biodegradable and Biobased Polyesters: Polymorphism, Cocrystallization, and Structure-Property Relationship. *Prog. Polym. Sci.* **2020**, *109*, No. 101291.
- (3) Chen, Q.; Auras, R.; Uysal-Unalan, I. Role of Stereocomplex in Advancing Mass Transport and Thermomechanical Properties of Poly(lactide). *Green Chem.* **2022**, *24*, 3416–3432, DOI: [10.1039/D1GC04520B](https://doi.org/10.1039/D1GC04520B).
- (4) Tsuji, H. Poly(Lactic Acid) Stereocomplexes: A Decade of Progress. *Adv. Drug Delivery Rev.* **2016**, *107*, 97–135.
- (5) Lee, S.; Kimoto, M.; Tanaka, M.; Tsuji, H.; Nishino, T. Crystal Modulus of Poly (Lactic Acid)S, and Their Stereocomplex. *Polymer* **2018**, *138*, 124–131.
- (6) Sangroniz, A.; Chaos, A.; Iriarte, M.; del Río, J.; Sarasua, J.-R.; Etxeberria, A. Influence of the Rigid Amorphous Fraction and Crystallinity on Polylactide Transport Properties. *Macromolecules* **2018**, *51* (11), 3923–3931.
- (7) Di Lorenzo, M. L.; Righetti, M. C. Crystallization-Induced Formation of Rigid Amorphous Fraction. *Polym. Cryst.* **2018**, *1* (2), No. e10023.
- (8) Tsuji, H.; Tsuruno, T. Water Vapor Permeability of Poly(L-Lactide)/Poly(D-Lactide) Stereocomplexes. *Macromol. Mater. Eng.* **2010**, *295* (8), 709–715.
- (9) Gupta, A.; Mulchandani, N.; Shah, M.; Kumar, S.; Katiyar, V. Functionalized Chitosan Mediated Stereocomplexation of Poly(Lactic Acid): Influence on Crystallization, Oxygen Permeability, Wettability and Biocompatibility Behavior. *Polymer* **2018**, *142*, 196–208.
- (10) Xu, H.; Wu, D.; Yang, X.; Xie, L.; Hakkarainen, M. Thermostable and Impermeable “Nano-Barrier Walls” Constructed by Poly(Lactic Acid) Stereocomplex Crystal Decorated Graphene Oxide Nanosheets. *Macromolecules* **2015**, *48* (7), 2127–2137.
- (11) Safandowska, M.; Makarewicz, C.; Rozanski, A.; Idczak, R. Barrier Properties of Semicrystalline Poly(lactide): The Role of the Density of the Amorphous Regions. *Macromolecules* **2022**, *55* (22), 10077–10089.
- (12) Limsukon, W.; Auras, R.; Smith, T. Effects of the Three-Phase Crystallization Behavior on the Hydrolysis of Amorphous and Semicrystalline Poly(Lactic Acid)S. *ACS Appl. Polym. Mater.* **2021**, *3* (11), 5920–5931.

- (13) Kanehashi, S.; Kusakabe, A.; Sato, S.; Nagai, K. Analysis of Permeability; Solubility and Diffusivity of Carbon Dioxide; Oxygen; and Nitrogen in Crystalline and Liquid Crystalline Polymers. *J. Membr. Sci.* **2010**, *365* (1), 40–51.
- (14) Gedde, U. W.; Unge, M.; Nilsson, F.; Hedenqvist, M. S. Mass and Charge Transport in Polyethylene – Structure, Morphology and Properties. *Polymer* **2023**, *266*, No. 125617.
- (15) Hu, Y. S.; Liu, R. Y. F.; Zhang, L. Q.; Rogunova, M.; Schiraldi, D. A.; Nazarenko, S.; Hiltner, A.; Baer, E. Oxygen Transport and Free Volume in Cold-Crystallized and Melt-Crystallized Poly(Ethylene Naphthalate). *Macromolecules* **2002**, *35* (19), 7326–7337.
- (16) Guinault, A.; Sollogoub, C.; Ducruet, V.; Domenek, S. Impact of Crystallinity of Poly(Lactide) on Helium and Oxygen Barrier Properties. *Eur. Polym. J.* **2012**, *48* (4), 779–788.
- (17) Sonchaeng, U.; Iniguez-Franco, F.; Auras, R.; Selke, S.; Rubino, M.; Lim, L. T. Poly(Lactic Acid) Mass Transfer Properties. *Prog. Polym. Sci.* **2018**, *86*, 85–121.
- (18) Pan, P.; Yang, J.; Shan, G.; Bao, Y.; Weng, Z.; Cao, A.; Yazawa, K.; Inoue, Y. Temperature-Variable Ftir and Solid-State ¹³C Nmr Investigations on Crystalline Structure and Molecular Dynamics of Polymorphic Poly(L-Lactide) and Poly(L-Lactide)/Poly(D-Lactide) Stereocomplex. *Macromolecules* **2012**, *45* (1), 189–197.
- (19) Fernandes Nassar, S.; Guinault, A.; Delpouve, N.; Divry, V.; Ducruet, V.; Sollogoub, C.; Domenek, S. Multi-Scale Analysis of the Impact of Polylactide Morphology on Gas Barrier Properties. *Polymer* **2017**, *108*, 163–172.
- (20) Michaels, A. S.; Bixler, H. J. Flow of Gases through Polyethylene. *J. Polym. Sci.* **1961**, *50* (154), 413–439.
- (21) Cocca, M.; Di Lorenzo, M. L.; Malinconico, M.; Frezza, V. Influence of Crystal Polymorphism on Mechanical and Barrier Properties of Poly(L-Lactic Acid). *Eur. Polym. J.* **2011**, *47* (5), 1073–1080.
- (22) Zhang, M.; Fan, X.; Guo, W.; Zhou, H.; Li, Z.; Ma, Y.; Yan, C.; Dufresne, A. Insights into Stereocomplexation of Poly(Lactic Acid) Materials: Evolution of Interaction between Enantiomeric Chains and Its Role in Conformational Transformation in Racemic Blends. *ACS Appl. Polym. Mater.* **2022**, *4* (8), 5891–5900.
- (23) Pan, P.; Han, L.; Bao, J.; Xie, Q.; Shan, G.; Bao, Y. Competitive Stereocomplexation, Homocrystallization, and Polymorphic Crystalline Transition in Poly(L-Lactic Acid)/Poly(D-Lactic Acid) Racemic Blends: Molecular Weight Effects. *J. Phys. Chem. B* **2015**, *119* (21), 6462–6470.
- (24) Tsuji, H.; Tezuka, Y. Stereocomplex Formation between Enantiomeric Poly(Lactic Acid)S. 12. Spherulite Growth of Low-Molecular-Weight Poly(Lactic Acid)S from the Melt. *Biomacromolecules* **2004**, *5* (4), 1181–1186.
- (25) Shao, J.; Xiang, S.; Bian, X.; Sun, J.; Li, G.; Chen, X. Remarkable Melting Behavior of Pla Stereocomplex in Linear Plla/Pdla Blends. *Ind. Eng. Chem. Res.* **2015**, *54* (7), 2246–2253.
- (26) Di Lorenzo, M. L.; Androsch, R. Influence of Alpha [′]-/Alpha-Crystal Polymorphism on Properties of Poly(L-Lactic Acid). *Polym. Int.* **2019**, *68* (3), 320–334.
- (27) Aliotta, L.; Cinelli, P.; Coltelli, M. B.; Righetti, M. C.; Gazzano, M.; Lazzeri, A. Effect of Nucleating Agents on Crystallinity and Properties of Poly(Lactic Acid) (Pla). *Eur. Polym. J.* **2017**, *93*, 822–832.
- (28) Chen, Q.; Auras, R.; Corredig, M.; Kirkensgaard, J. J. K.; Mamakhel, A.; Uysal-Unalan, I. New Opportunities for Sustainable Bioplastic Development: Tailorable Polymorphic and Three-Phase Crystallization of Stereocomplex Polylactide by Layered Double Hydroxide. *Int. J. Biol. Macromol.* **2022**, *222*, 1101–1109.
- (29) Leng, J.; Purohit, P. J.; Kang, N.; Wang, D.-Y.; Falkenhagen, J.; Emmerling, F.; Thünemann, A. F.; Schönhals, A. Structure–Property Relationships of Nanocomposites Based on Polylactide and MgAl Layered Double Hydroxides. *Eur. Polym. J.* **2015**, *68*, 338–354.
- (30) Sangroniz, A.; Sarasua, J. R.; Iriarte, M.; Etxeberria, A. Survey on Transport Properties of Vapours and Liquids on Biodegradable Polymers. *Eur. Polym. J.* **2019**, *120*, No. 109232.
- (31) Du, A.; Koo, D.; Therey, G.; Hillmyer, M. A.; Cairncross, R. A. Water Transport and Clustering Behavior in Homopolymer and Graft Copolymer Poly(lactide). *J. Membr. Sci.* **2012**, *396*, 50–56.
- (32) Auras, R.; Harte, B.; Selke, S. Effect of Water on the Oxygen Barrier Properties of Poly(Ethylene Terephthalate) and Polylactide Films. *J. Appl. Polym. Sci.* **2004**, *92* (3), 1790–1803.
- (33) Davis, E. M.; Elabd, Y. A. Prediction of Water Solubility in Glassy Polymers Using Nonequilibrium Thermodynamics. *Ind. Eng. Chem. Res.* **2013**, *52* (36), 12865–12875.
- (34) Pannico, M.; La Manna, P. Sorption of Water Vapor in Poly(L-Lactic Acid): A Time-Resolved Ftir Spectroscopy Investigation. *Front. Chem.* **2019**, *7*, No. 275, DOI: 10.3389/fchem.2019.00275.
- (35) Di Lorenzo, M. L.; Cocca, M.; Malinconico, M. Crystal Polymorphism of Poly(L-Lactic Acid) and Its Influence on Thermal Properties. *Thermochim. Acta* **2011**, *522* (1–2), 110–117.
- (36) Di Lorenzo, M. L.; Righetti, M. C.; Wunderlich, B. Influence of Crystal Polymorphism on the Three-Phase Structure and on the Thermal Properties of Isotactic Poly(1-Butene). *Macromolecules* **2009**, *42* (23), 9312–9320.
- (37) Righetti, M. C.; Tombari, E. Crystalline, Mobile Amorphous and Rigid Amorphous Fractions in Poly(L-Lactic Acid) by Tmdsc. *Thermochim. Acta* **2011**, *522* (1), 118–127.
- (38) Parodi, E.; Govaert, L. E.; Peters, G. W. M. Glass Transition Temperature Versus Structure of Polyamide 6: A Flash-Dsc Study. *Thermochim. Acta* **2017**, *657*, 110–122.
- (39) Barrer, R. M.; Barrie, J. A.; Slater, J. Sorption and Diffusion in Ethyl Cellulose. Part Iii. Comparison between Ethyl Cellulose and Rubber. *J. Polym. Sci.* **1958**, *27* (115), 177–197.
- (40) Vieth, W. R.; Tam, P. M.; Michaels, A. S. Dual Sorption Mechanisms in Glassy Polystyrene. *J. Colloid Interface Sci.* **1966**, *22* (4), 360–370.
- (41) Li, P.; Chung, T. S.; Paul, D. R. Gas Sorption and Permeation in Pim-1. *J. Membr. Sci.* **2013**, *432*, 50–57.
- (42) Kamiya, Y.; Naito, Y.; Terada, K.; Mizoguchi, K.; Tsuboi, A. Volumetric Properties and Interaction Parameters of Dissolved Gases in Poly(Dimethylsiloxane) and Polyethylene. *Macromolecules* **2000**, *33* (8), 3111–3119.
- (43) Jordan, S. S.; Koros, W. J. A Free Volume Distribution Model of Gas Sorption and Dilatation in Glassy Polymers. *Macromolecules* **1995**, *28* (7), 2228–2235.
- (44) Paul, D. R. Gas Sorption and Transport in Glassy Polymers. *Ber. Bunsengesellschaft Phys. Chem.* **1979**, *83* (4), 294–302.
- (45) Díez-Rodríguez, T. M.; Blázquez-Blázquez, E.; Martínez, J. C.; Pérez, E.; Cerrada, M. L. Composites of a Pla with Sba-15 Mesoporous Silica: Polymorphism and Properties after Isothermal Cold Crystallization. *Polymer* **2022**, *241*, No. 124515.
- (46) Díez-Rodríguez, T. M.; Blázquez-Blázquez, E.; Martínez, J. C.; Cerrada, M. L.; Pérez, E. A Synchrotron Saxs Study of Plla Crystallized at Different Temperatures: One-Dimensional Correlation Functions. *Polymer* **2022**, *256*, No. 125232.
- (47) Zhang, L.; Zhao, G.; Wang, G. Investigation on the A/Δ Crystal Transition of Poly(L-Lactic Acid) with Different Molecular Weights. *Polymers* **2021**, *13* (19), 3280.
- (48) Wasanasuk, K.; Tashiro, K. Crystal Structure and Disorder in Poly(L-Lactic Acid) Δ Form (A′ Form) and the Phase Transition Mechanism to the Ordered A Form. *Polymer* **2011**, *52* (26), 6097–6109.
- (49) Kalish, J. P.; Zeng, X.; Yang, X.; Hsu, S. L. A Spectroscopic Analysis of Conformational Distortion in the A′ Phase of Poly(Lactic Acid). *Polymer* **2011**, *52* (15), 3431–3436.
- (50) Wasanasuk, K.; Tashiro, K.; Hanesaka, M.; Ohhara, T.; Kurihara, K.; Kuroki, R.; Tamada, T.; Ozeki, T.; Kanamoto, T. Crystal Structure Analysis of Poly(L-Lactic Acid) A Form on the Basis of the 2-Dimensional Wide-Angle Synchrotron X-Ray and Neutron Diffraction Measurements. *Macromolecules* **2011**, *44* (16), 6441–6452.
- (51) Esposito, A.; Delpouve, N.; Causin, V.; Dhotel, A.; Delbreilh, L.; Dargent, E. From a Three-Phase Model to a Continuous Description of Molecular Mobility in Semicrystalline Poly-

(Hydroxybutyrate-Co-Hydroxyvalerate). *Macromolecules* **2016**, *49* (13), 4850–4861.

(52) Gavara, R.; Hernandez, R. J. Consistency Test for Continuous Flow Permeability Experimental Data. *J. Plast. Film Sheeting* **1993**, *9* (2), 126–138.

(53) Tsujita, Y. Gas Sorption and Permeation of Glassy Polymers with Microvoids. *Prog. Polym. Sci.* **2003**, *28* (9), 1377–1401.

(54) Koros, W. J.; Paul, D. R. Observations Concerning the Temperature Dependence of the Langmuir Sorption Capacity of Glassy Polymers. *J. Polym. Sci., Polym. Phys. Ed.* **1981**, *19* (10), 1655–1656.

(55) Lin, W.-H.; Chung, T.-S. Gas Permeability, Diffusivity, Solubility, and Aging Characteristics of 6FDA-Durene Polyimide Membranes. *J. Membr. Sci.* **2001**, *186* (2), 183–193.